Electronics and Electrical Engineering

AIMS Electronics and Electrical Engineering, 8(4): 478–497.
DOI: 10.3934/electreng.2024023
Received: 17 March 2024
Revised: 08 October 2024
Accepted: 05 November 2024
Published: 22 November 2024

http://www.aimspress.com/journal/ElectrEng

Research article

Microwave-assisted heating in a novel thin film-liquid spinning coaxial reactor

Guennadi A. Kouzaev*

Department of Electronic Systems, Norwegian University of Science and Technology, Trondheim, 7491 Norway

* **Correspondence:** Email: guennadi.kouzaev@ntnu.no; kouzaev@hotmail.com.

Abstract: This paper introduces a novel rotating reactor designed for microwave-assisted heating and chemical processes. It consists of a sealed coaxial waveguide with a dielectric hollow mixer that rotates along the length of the central conductor. A heating liquid flows in a narrow gap between this rotor and the outer shield of the coaxial waveguide, powered by microwaves. It is hypothesized that the acceleration of the conversation rate of chemical reactions is due to the excitation of micro-vortices for better mixing and the direct application of microwaves to a mix of polar reagents within the narrow gap. This study presents initial experimental results of microwave liquid heating, hydrodynamics, and mechanics in this reactor.

Keywords: continuous-flow chemistry; spinning chemical reactors; microwave-assisted heating; microwave coaxial spinning reactors

1. Introduction

The development of green chemistry technologies requires new processes and hardware, allowing increased conversion rates, improved product selectivity and yields, enhanced safety conditions, decreased energy usage, and low product cost [1–4]. These technologies often include systems controlled through wireless networks in human-free conditions. For instance, there is significant interest in launching chemical laboratories into space for enhanced synthesis of biochemical products [5–7].

Accelerating chemical processes can be reached by different means, guided by a modified Arrhenius equation [8]:

$$K = \rho Z_{AB}(T)\exp(-E_a/RT) \tag{1}$$

where K is the rate constant, i.e., frequency of collisions resulting in a reaction, and ρ is the steric factor depending on the shape of interacting molecules A and B and their orientations at a collision. Z_{AB} is the number of binary collisions of molecules A and B, E_a is the chemical reaction activation energy, R is the Avogadro constant, and T is the absolute temperature. It is clear that the main influencing factor of the reaction rate is temperature.

Another critical factor is the number of collisions $Z_{AB}(T)$, dependent on the delivery of molecules to the interaction points. This is achieved by preliminary mixing of reagents in a solvent using laminar, non-laminar, diffusion, or boiling flows in batch chemistry.

Rotational mixing is routinely used in liquid chemistry [9,10]. Among these devices are tube-in-tube reactors, distinguished by increased conversion rates. They are built on an inner rotating cylinder inserted into another stator tube. The heated mixture is pumped between the two mentioned cylinders. If the mixture's viscosity is relatively high and the gap is large enough, Taylor-Couette vortices are generated along the reactor, facilitating better mixing and increasing the conversion rate [9–13].

Different designs have been proposed for thin-film liquid tube-in-tube reactors [9,12–14]. These reactors pump fluids in a narrow sub-millimeter gap, allowing the generation of micrometric vortices for fine mixing of externally heated reagents.

On the contrary, microwave (MW)-assisted chemistry involves heating polar liquids directly in reactors [10,15,16]. Unfortunately, the conventional MW ovens based on hollow cavities are unsuitable for tailored chemistry because of their employed frequency of 2.45 GHz; they also require a large amount of energy, even for synthesis in small vials. Miniature and energy-efficient MW reactors can be built on transversal electromagnetic (TEM) waveguides and semiconductor generators. Some designs use coaxial waveguides [17–29], which allow scalability [18,20]. For high-loss liquids, the residence time in reactors is increased with dielectric-layered quasi-TEM coaxial waveguides [26,28].

MW coaxial designs are well-suited for rotating thin-film liquid reactors. The first device of this kind was proposed in [29], featuring a central conductor inserted into a hollow dielectric rotor. The liquid flows in the narrow gap between this rotor and the outer shield under MW heating. Enhanced conversion rates are expected due to improved mixing by exciting the sub-millimeter liquid vortices in the narrow gap [9] and specific MW effects in microchannels [30].

This paper aims to confirm the workability of the design proposed in [29] and investigate key effects and challenges for optimizing the thin-film MW-assisted spinning coaxial reactors.

2. Microwave spinning coaxial reactor

One of the developed devices, Kinel-2.0, is shown in Figures 1 and 2. It consists of a spool-like coaxial reactor with installed alumina (Appendix, Table 1A, row 1) or quartz (Table 1A, row 2) tube, closed at one end and rotating around the central conductor (shown in black in Figure 2) using a flexible coupler by an electromotor (Table 1A, row 3). This wire conductor extends inside the tube to a length H_c and serves as an open-end applicator, heating the liquid as it moves from the inlet to

the outlet through the circular slot between the spinning rotor and coaxial shield (Figure 2). The slot size (<1 mm) and rotation speed $(\approx 3\,000 - 4\,000$ rpm$)$ were chosen according to literature data [9,12–14] on non-microwave spinning reactors.

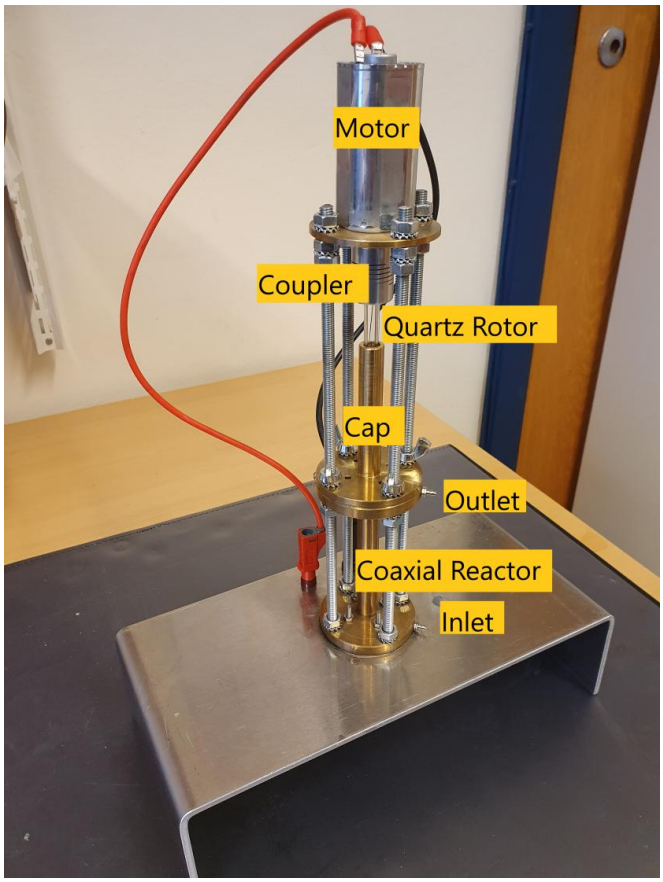

Figure 1. MW thin-film liquid spinning coaxial reactor Kinel 2.0.

This reactor is fed by MWs from below the board using a coaxial connector (Table 1A, row 4). Rubber rings (shown in blue in Figure 2) seal this reactor from both ends, and the caps support a certain pressure to ensure hermeticity. Wetting of the upper ring is achieved by maintaining the required liquid pressure internally and/or with liquid provided through the circular cap slot between the rotor and the cap wall.

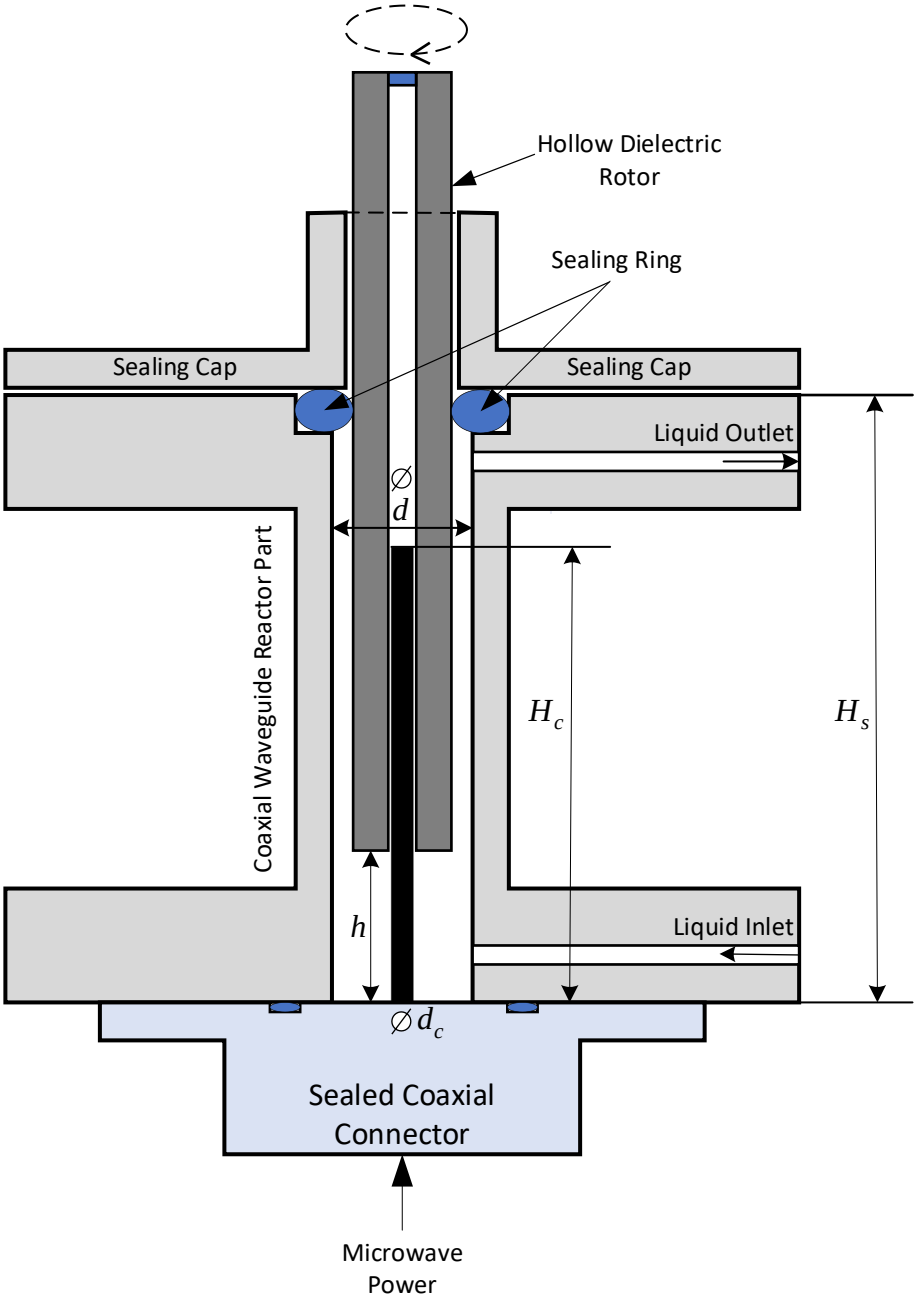

Figure 2. MW spinning coaxial reactor Kinel 2.0 with the following geometrical parameters: $H_s = 100$ mm, $H_c = 85$ mm, $h = \text{var}$, $d = 8$ mm, and $d_c = 2$ mm.

Microwaves are initially excited in the reactor through the mentioned sealed coaxial connector in the cavity below the rotor end (Figure 2) as a transverse electromagnetic (TEM) wave. The wave then travels to the partially filled coaxial waveguide. Its cross-section is mainly occupied by the dielectric rotor. This waveguide's primary mode is a quasi-TEM type. This wave is reflected from the end of the central rod, and power partially comes to the layered lossy circular waveguide, whose size dampens the propagation of its main mode. The cross-sections of the inlet/outlet channels are too small for wave propagation.

3. Measurement setup

Figures 3 (block diagram) and 4 (physical implementation) illustrate the setup for measuring the temperature of liquids in MW spinning reactors. All commercially available component data are given in Appendix, Table 1A.

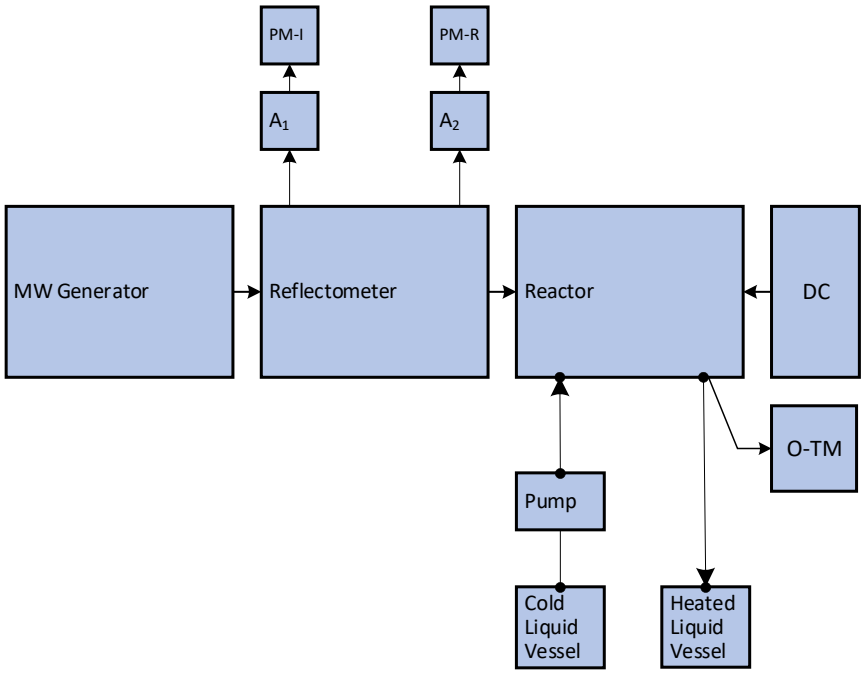

Figure 3. Block diagram of the measurement setup for thermal characterization of MW-assisted heating of liquids in coaxial spinning reactors. A_1 and A_2 are the attenuators, and PM-I and PM-R are the power meters for measuring the MW generator's and reflected reactor's powers. O-TM is an optical fiber thermometer.

The setup consists of an MW generator (Table 1A, row 5) whose power can be adjusted from 0 to 250 W in 10 W increments, controlled by a computer. Approximate output data and reflected power values are available directly from this generator. More accurate power measurement results are available in the reflectometer (Table 1A, row 6), which samples small portions of the generator's and reflected powers, relayed through coaxial cables (Table A1, row 7) to power meters PM-I and PM-R (Table 1A, rows 8 and 9). Unfortunately, this generator lacks fine-tuning capabilities for precise power adjustment using its digital interface. Besides, like most high-power generators and amplifiers, it may show some thermal noise and power level drift, especially in multi-hour experiments. Nevertheless, this instrument, intended for MW heating, provided acceptable performance in our research.

The attenuators A_1 and A_2 (Table 1A, rows 10 and 11) adjust the incoming levels for accurate measurements. A coaxial cable connects the reflectometer to the reactor (Table 1A, row 12). A polar liquid from vessel 1 reaches the reactor using a pump (Table 1A, row 13) and tubing (Table 1A, row 14). At the outlet, the temperature is measured by an optic fiber thermometer (O-TM; Table 1A, row 15), whose sensor is installed directly in the reactor cavity near the rotating dielectric cylinder. This sensor is not influenced by MW irradiation.

The heated liquid is evacuated to a glass vessel 2 using Tygon tubing. A DC source (24 V) of a regulated and controlled current (0–15 A) feeds the reactor's electromotor. The speed of dielectric rotors is measured using a non-contact tachometer (Table 1A, row 16).

The level of possible parasitic MW irradiation is measured by a power indicator (Table 1A, row 17). Observed levels were significantly below the maximum allowed power density of 5 mW/cm^2, even close to the reactor and connectors during heating experiments.

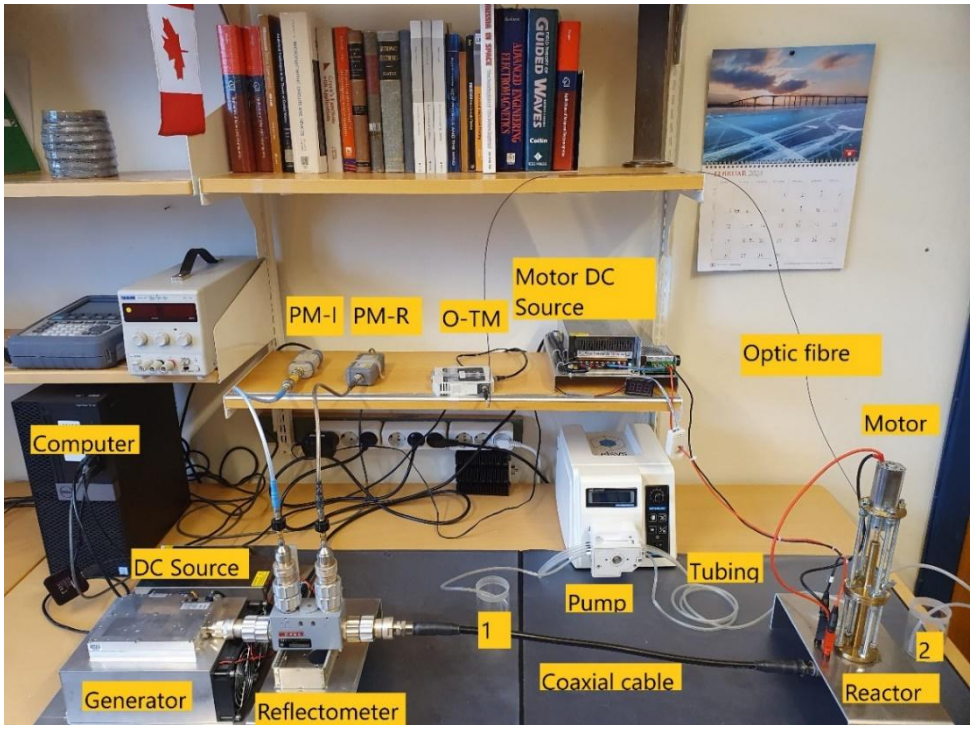

Figure 4. Measurement setup for MW-assisted liquid heating in a spinning coaxial reactor. The vessels for cold and heated liquids are marked by 1 and 2, respectively.

The frequency properties of the reactors filled with ethanol (Table 1A, row 18) and methanol (Table 1A, row 19) at room temperature were analyzed preliminary using a network analyzer (Table 1A, row 20). The last three instruments are not shown in Figures 3 and 4.

All experiments were performed at the Department's Chemical Laboratory, equipped with air-hood chambers and safety hardware.

4. Materials and components

Details and characteristics of all used materials and components are given in Tables 1, 2, and Appendix 1A.

4.1. Reference liquids

As reference liquids, ethanol (C_2H_5OH) and methanol (CH_3OH) were used [31,32]. The dielectric parameters of these liquids depend on frequency and temperature. At 2.5 GHz and 20 ℃,

the complex relative permittivity of ethanol is $\tilde{\varepsilon}_{\mathrm{ET}}^{(r)} \approx 6.59 - j6.30$; for methanol, this parameter is $\tilde{\varepsilon}_{(\mathrm{MT})}^{(r)} \approx 21.30 - j13.88$ [31]. The first one is more lossy due to comparable real and imaginary permittivity components.

The parameters mentioned above depend on the inner structure of the alcohol molecules and their interactions with each other. For instance, ethanol molecules' polarity is weaker than methanol due to longer carbon chains, resulting in a lower real permittivity. Ethanol has six hydrogen atoms, which can be coupled to neighboring molecules. The boiling point of ethanol (78.23 ℃) is higher than that of methanol (64.7 ℃), which has only four hydrogen atoms. These interactions define other parameters of these liquids, as shown in Table 1.

Table 1. Parameters of used reference liquids.

Liquid	Complex relative dielectric permittivity and $\tan\delta$, at 25 °C	Boiling point, t_{B}, °C	Specific heat capacity, C_V J/(mol K)	Viscosity, mPa·s, at 25 °C
Ethanol, C_2H_5OH	7.10-*j*6.83, $\tan\delta = 0.96$	78.23	100	1.074
Methanol, CH_3OH	22.13-*j*13.20, $\tan\delta = 0.6$	64.7	81.08	0.545

4.2. Reactor materials

In this paper, the developed reactor was made of brass, whose specific electric conductivity is 28% that of copper (5.96×10^7 Sim/m). The central conductor was stainless steel (1.45×10^7 Sim/m), chosen for its mechanical strength. The rotors are made from alumina ceramic or quartz. Their electric parameters are shown in Table 2.

Table 2. Electric parameters of rotor materials.

Rotor material	Dielectric relative permittivity, ε_r	Dielectric loss tangent, $\tan\delta$
Rotor 1, alumina, Al_2O_3	9.9	0.0001
Rotor 2, fused quartz, SiO_2	3.78	2×10^6

5. Results

5.1. Practical matching of reactors

The design is based on an open-end central conductor of a coaxial waveguide (Figure 2). Untuned reactors have increased reflection [32,33]. Some additional mismatching occurs due to the parasitics from connectors, reflectometers, and cables, as well as due to the temperature drift of dielectric parameters of heated liquids [32]. The narrow bandwidth matching leads to transients near generator activation. Due to the inertia of the heating process, slight variations of incident power during the heating process do not influence the temperature of a liquid at the outlet.

Reactors can be matched using the outer mechanicalor electromechanical tuners or by varying the geometry of heaters [32]. Particularly, in [33], a technique was used to change the rotor's immersed length inside the spool reactor (Figure 2) when filled with a liquid at room temperature.

In this experiment, two different rotors were used. One is made of alumina (Table 1A, row 1), and another of quartz (Table 1A, row 2). A calibrated network analyzer is connected directly to the reactor filled with room-temperature liquid. Measurements show that the untuned geometry $h = 0$ mm (see Figure 2) leads to strong reflection.

Similarly to [33], the tuning of the reactor is achieved by changing the height h of the mini-cavity below the dielectric rotor (Figure 2). Particularly, for an alumina tube, $h = 14$ mm was used; for quartz, $h = 10$ mm. In this case, the reflection coefficient calculated according to the measured power data ($P_{\mathrm{G}}\left(t, t^{\circ}\right)$ and $P_{\mathrm{ref}}\left(t, t^{\circ}\right)$) at the reflectometer ports (Figures 3 and 4) is within the 25%–35% limit (Figures 5–11), which is acceptable for the research of these reactors.

This simple technique has its advantages and disadvantages. For instance, the liquid-filled cavity below the rotor's end may hinder its geometrical scalability due to the complicated physics of multiphase-heated liquids. Outer matching may be preferable for finalized designs with a fixed minimal length of cavities below the end of the rotors.

5.2. Results of heating experiments

Temperature measurements of heated ethanol and methanol were performed at the reactor liquid outlet (Figures 2, 3). The rate of a ten-roller pump was supported at 1.5 mL/min for all measurements. The reactor was connected to this pump by a transparent Tygon tube of 1 m length to minimize the rest of the liquid pulsation originating from the peristaltic pumping. Each measurement starts with a preliminary cooled reactor at room temperature.

5.2.1. Heating experiments with ethanol and ceramic rotor reactor

Consider some results on ethanol heating in the reactor with a ceramic rotor. Initially, this device was studied in the static rotor regime, applying different generator power levels. For instance, the heating experiment for the generator power around 70 W is shown in Figure 5.

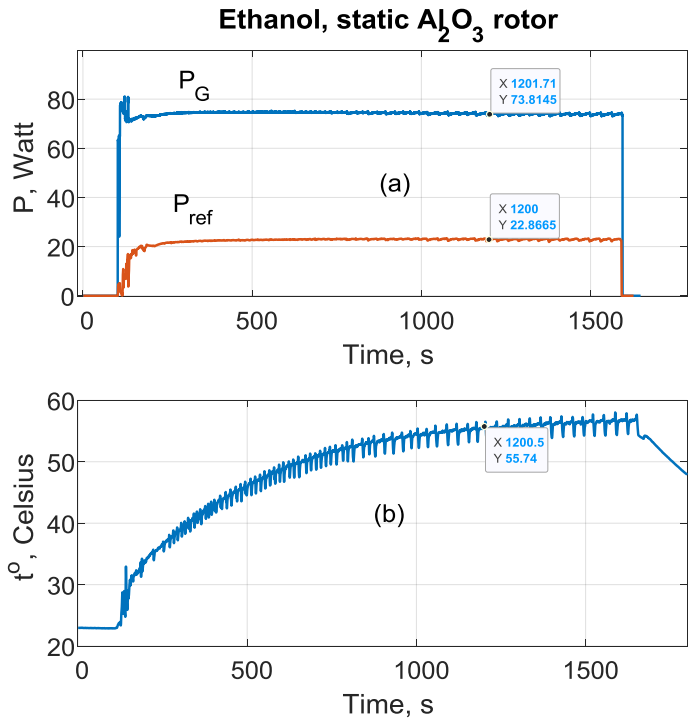

Figure 5. Ethanol heating experiments in the case of static ceramic rotor. (a) $P_G \approx 74$ W and P_{ref} are the generator and reflected power levels at the ports of the reflectometer (see Figures 3 and 4), respectively; (b) temperature trend measured in the liquid outlet channel close to its opening to the reactor volume (Figure 2).

Transient behavior is found in the applied and reflected power trends near the switching time of the generator (Figure 5(a)). An associated temperature jump is seen in Figure 5(b) with a slight delay, meaning that the liquid is heated by microwaves, even at the end of the reactor, close to the outlet tube.

Some quasiperiodic few-degree temperature oscillations (Figure 5b) occurred despite relatively steady power trends (Figure 5a). A similar behavior of the decreased magnitude was found for the lower applied power levels; this is shown in Figure 6, where the generator's power is around 60 W.

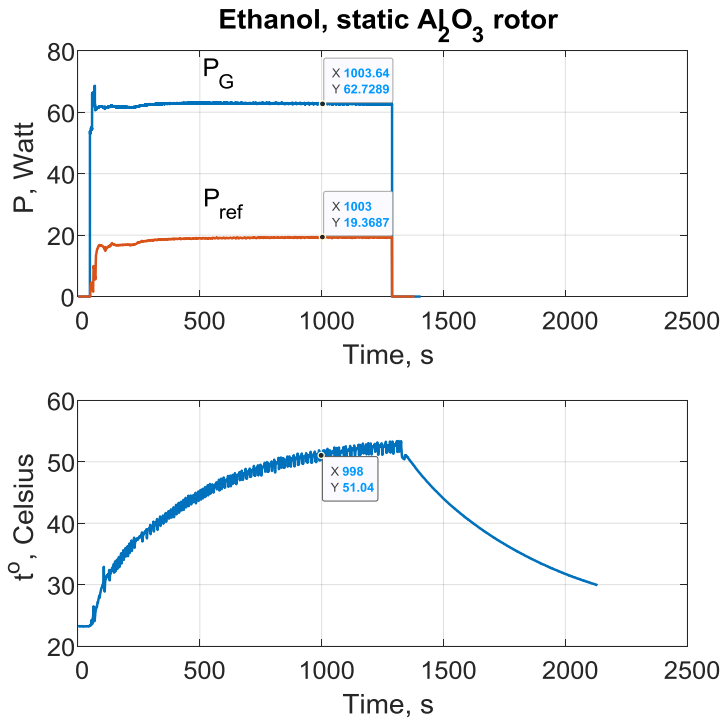

Figure 6. Ethanol heating experiments in the case of static ceramic rotor. (a) $P_G \approx 63$ W and P_{ref} are the generator and reflected power levels at the ports of the reflectometer (see Figures 3 and 4), respectively; (b) temperature trend measured in the liquid outlet channel close to its opening to the reactor volume.

The nature of these oscillations is not definitely known. One reason is intensive bubbling in the cavity below the rotor end, where the power density of the applied MW field is very high. Also, these bubbles are seen along the used outlet Tygon transparent tube, although the liquid temperature is reduced due to heat exchange with the reactor body. Similar behavior was found in [32], where the heating of liquids in plastic tubes was studied. Another possible cause is the overheating of liquids in the mentioned cavity and the slugged motion of overheated drops to the outlet.

These quasi-periodical effects diminished in the rotating regime, shown in Figure 7. Here, the reflected power is much noisier due to the non-ideal centering of the design.

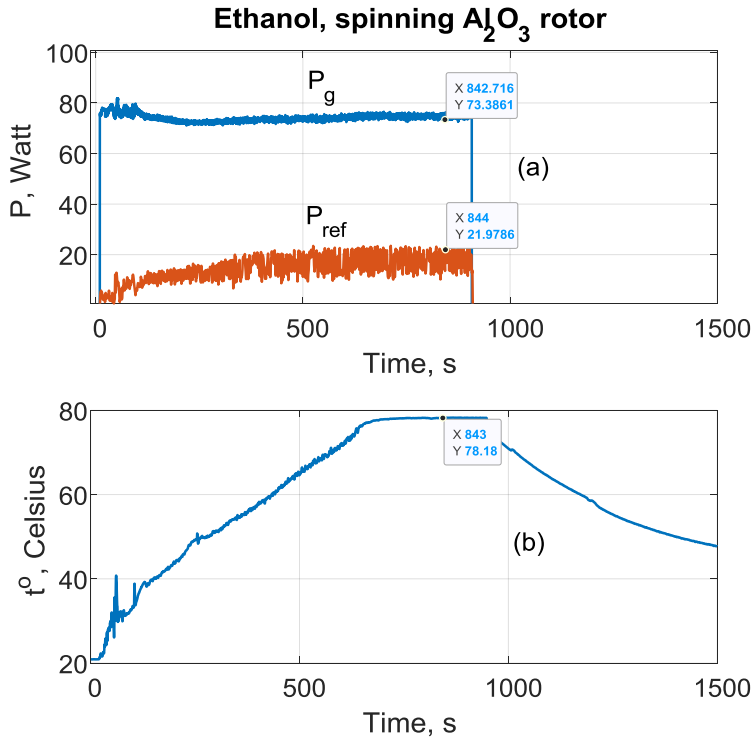

Figure 7. Ethanol heating experiments in the case of rotating ceramic rotor. (a) $P_G \approx$ 72-74 W and P_{ref} are the generator and reflected power levels at the ports of the reflectometer (see Figures 3 and 4), respectively; (b) temperature trend measured in the liquid outlet channel close to its opening to the reactor volume.

Despite the intensive generator's thermal noise arising after several hours of experiments, this temperature trend does not show the mentioned quasi-periodical oscillations explained by improved mixing ethanol in the cavity below the rotor and in the narrow cylindrical gap (0.5 mm) between the dielectric rotor and reactor wall (Figure 7). More research is required to precisely establish the nature of this quasi-periodical effect in temperature trends.

5.2.2. Heating experiments with methanol and ceramic rotor reactor

Similar experiments were performed with methanol. Figure 8 shows the power and temperature curves for the methanol-filled ceramic rotor reactor.

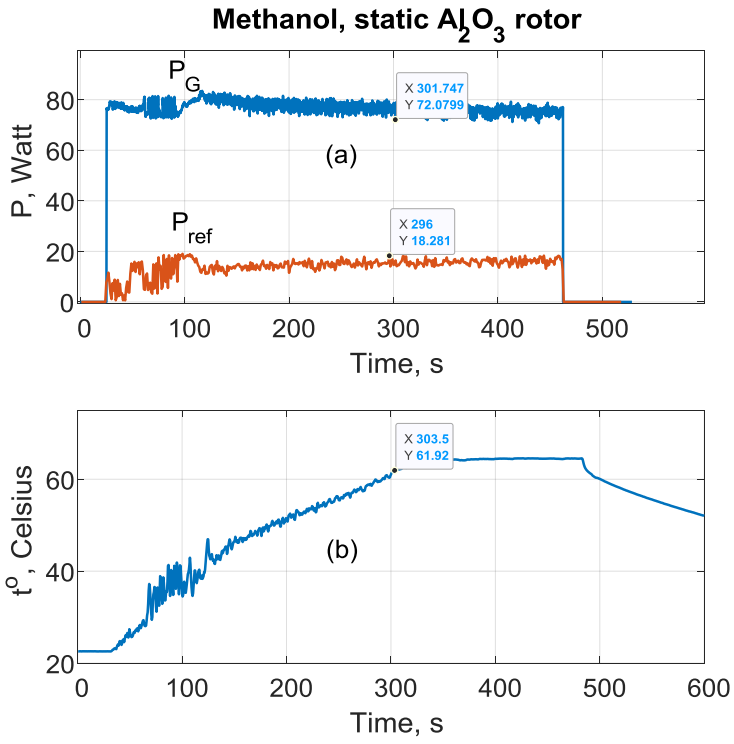

Figure 8. Methanol heating experiments in the case of static ceramic rotor. (a) $P_G \approx$ 80-72 W and P_{ref} are the generator and reflected power levels at the ports of the reflectometer (see Figures 3 and 4), respectively; (b) temperature trend measured in the liquid outlet channel close to its opening to the reactor volume.

Applying power around 80–72 W reaches the methanol boiling temperature measured at the outlet channel. In this case, the influence of bubbling on temperature is less visible. Still, the generator power is noisier than in Figure 5, and its level cannot be tuned precisely due to the generator design.

Figure 9 shows the methanol heating experiments with a spinning ceramic rotor. Methanol's trend pulsations are less influenced by the rotation than in Figure 6, mostly because this liquid has twice less viscosity than ethanol (Table 1). Excitation of micro-vortices is less effective in this case.

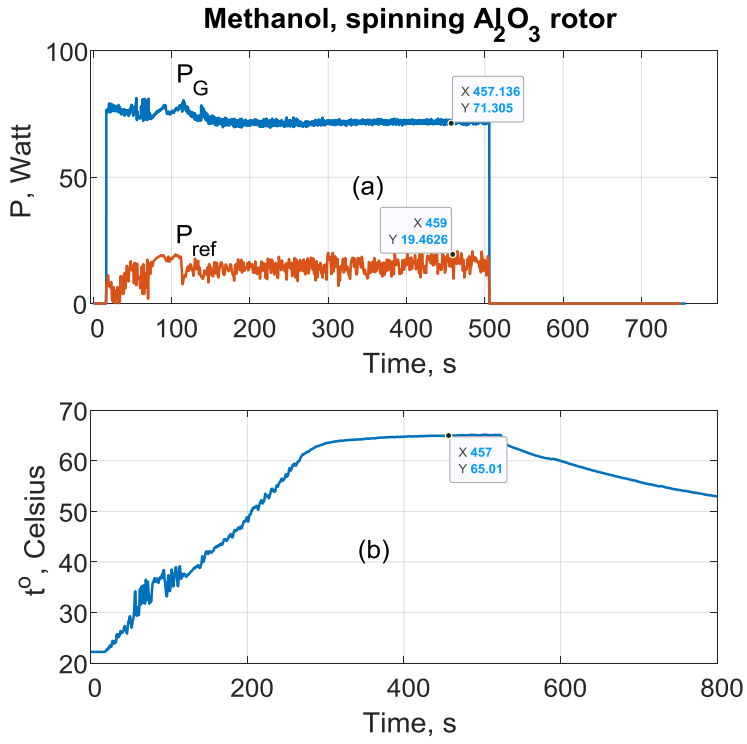

Figure 9. Methanol heating experiments in the case of rotating ceramic rotor. (a) $P_G \approx$ 80-71 W and P_{ref} are the generator and reflected power levels at the ports of the reflectometer (see Figures 3 and 4), respectively; (b) temperature trend measured in the liquid outlet channel close to its opening to the reactor volume.

In MW heating conditions, the temperature of liquids can surpass boiling temperature even at normal atmospheric pressure [32]. Figure 9 shows a similar effect that can be additionally strengthened by increasing liquid pressure inside the reactor and liquid degassing.

5.2.3. Heating experiments with ethanol and quartz rotor reactor

Some studies were performed with static (Figure 10) and rotating (Figure 11) quartz tubes and ethanol. Figure 10 shows the power (a) and temperature (b) trends for the static state of the quartz rotor. The behavior (occlusion effect) of liquid motion is similar to what was seen in Figure 5.

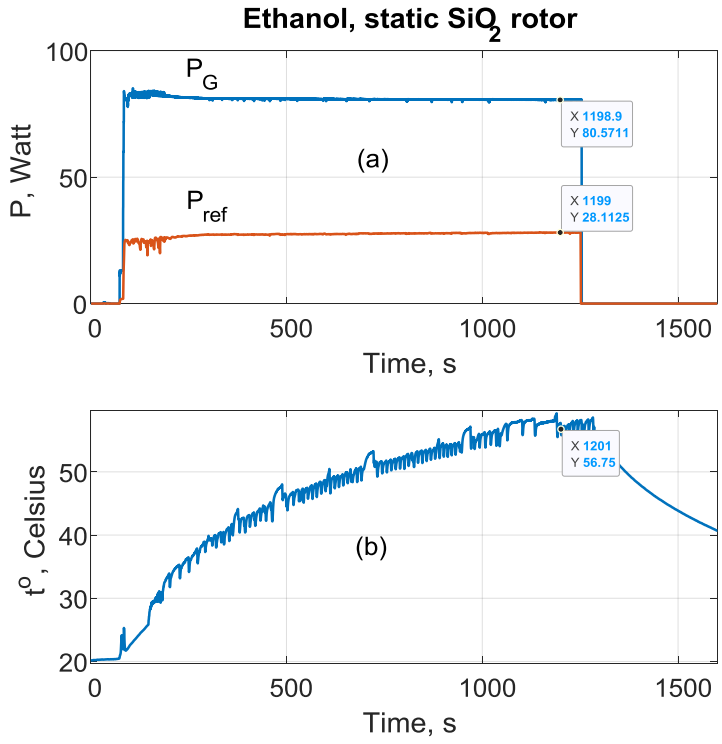

Figure 10. Ethanol heating experiments in the case of static quartz rotor. (a) $P_G \approx$85-80 and P_{ref} are the generator and reflected power levels at the ports of the reflectometer (see Figures 3 and 4), respectively; (b) temperature trend measured in the liquid outlet channel close to its opening to the reactor volume.

This occlusion effect is diminished in the rotating regime (Figure 11). By analyzing Figures 5 and 10, we need to consider the surface quality of alumina and quartz rotors; the first one has increased roughness (estimated visually), which may cause more effective excitation of liquid micro-vortices.

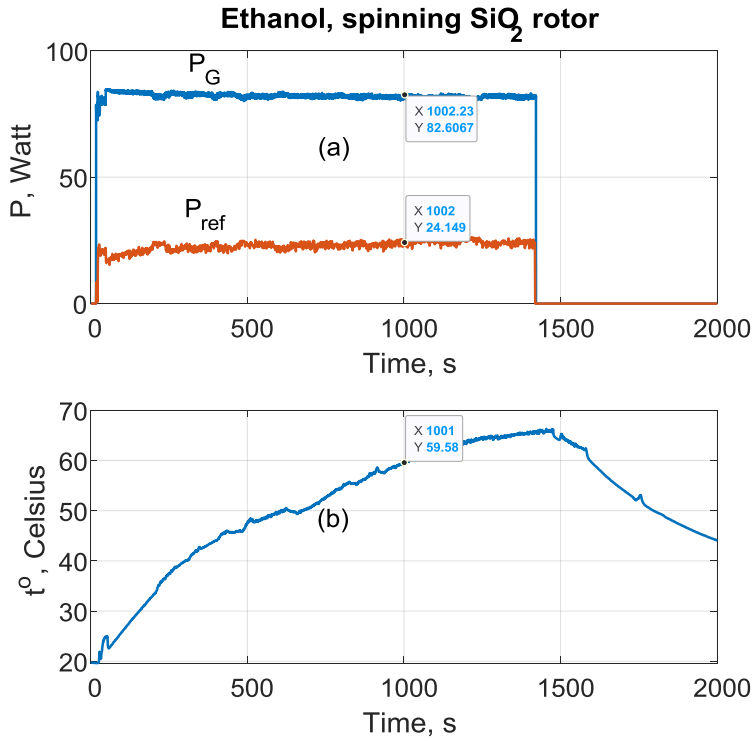

Figure 11. Ethanol heating experiment in the case of rotating quartz tube. (a) $P_G \approx$85-82 and P_{ref} are the generator and reflected power levels at the ports of the reflectometer (see Figures 3 and 4), respectively; (b) temperature trend measured in the liquid outlet channel close to its opening to the reactor volume.

6. Discussion

In this paper, a novel reactor was studied for liquid-heating experiments using a high-power MW generator, power meters, and an optic fiber thermometer resistant to MW irradiation. This study aimed to confirm the proposed reactor's workability in the dielectric rotor's static and spinning regime immersed in a sealed coaxial cavity [29,33]. This research was performed in realistic conditions, in which the high-power generator had limitations in fine-tuning power levels, some thermal noise, and power drift.

The manufactured reactor design also presented its own limitations in its MW and mechanical tuning. For instance, the used MW matching allowed only the regulation of the reactor reflection with the joined cables and connectors in a limited manner; ideally, it requires the outer tuners to adapt toward the input impedance temperature drift. In this case, the relatively large cavities with complicated two-phase liquid dynamics could be deleted from the design to improve the predictability of thermal processes.

Non-ideal centering may lead to vibration of the central rod of the coaxial cavity and a noise-like response of the reflected power (see Figures 7 and 9). This vibration can be diminished by better centering using PTFE bearings. Using massive metallic parts of the reactor body exposed to convective air leads to slow warming of the flowing liquids in the thin channel between the rotor and the coaxial outer shield. Glass-metal technology can alleviate this problem [27,28].

Nevertheless, the studied reactor showed stable heating of ethanol and methanol in the static

and spinning regimes of ceramic and quartz rotors. Spinning rotors damped the slugging effects and destroyed large bubbles of liquid vapor in the mentioned channel. The proposed design is open to moderate scalability if an outer tuning is applied without keeping large cavities below the rotor's end.

7. Conclusions

In this work, a novel microwave thin-film liquid spinning coaxial reactor was developed, manufactured, and studied in heating experiments. It consists of a coaxial vessel sealed from both ends, where the central conducting rod is installed into a hollow dielectric rotor with a regulated immersion length. This coaxial vessel is excited from the one end by microwaves using a sealed connector. The liquids are pumped to the reactor and following further to the sub-millimeter cylindrical gap between the stator (outer conductor of a coaxial waveguide) and dielectric rotor and heated. While the dielectric cylinder is rotating at high speed (2000–4000 rpm), fine turbulent flow arises due to the interaction of liquids with the rotating dielectric surface, which improves the mixing of reagents as shown in known non-microwave reactors of this type [9].

The experiments with MW-assisted heating ethanol and methanol confirmed the workability of the proposed device in the static and spinning regimes of the alumina and quartz rotors. For instance, rotating dampens the occlusion effect when the liquid flow is slugged and liquid drops are moving fast under the vapor pressure. Further design and developments will be done to enhance these reactors, with numerical simulations and experimental heating studies in different regimes, including analyzing bubbling and overheating effects. The scalability of this hardware should also be investigated.

The thin-film liquid spinning coaxial reactors are promising for rapid chemical synthesis where acceleration is achieved due to the fine mixing of reagents [9] and specific MW effects in sub-millimeter channels [30]. Assessing these reactors in increased safety environment applications, including space applications [5,6], is also fascinating.

Acknowledgments

The Author thanks the Small-Scale Project Fund (Information Technology and Electrical Engineering Faculty, NTNU) for financial support and Dr. S. Pettersen for his help in Chemical Laboratory.

He thanks the unknown reviewers for their critiques and advice.

Conflict of interest

The author declares that there is no conflict of interest in this paper.

References

1. Kitson PJ, Marie G, Francoia JP, Zalesskiy SS, Sigerson RC, Mathieson JS, et al. (2018) Digitization of multistep organic synthesis in reactionware for on-demand pharmaceuticals. *Science* 359: 314–319. https://doi.org/10.1126/science.aao3466

2. Li J, Ballmer S, Gillis E, Fujii S, Schmidt M, Palazzolo A, et al. (2015) Synthesis of many different types of small organic molecules using one automated process. *Science* 347: 1221–1226. https://doi.org/10.1126/science.aaa5414
3. Mascia S, Heider P, Zhang H (2013) End-to-end continuous manufacturing of pharmaceuticals: integrated synthesis, purification, and final dosage formation. *Angew Chem Int Ed* 52: 12359–12363. https://doi.org/10.1002/anie.201305429
4. Yang H, Yan B, Chen W, Fan D (2023) Prediction and innovation of sustainable continuous flow microwave processing based on numerical simulations: A systematic review. *Renewable and Sustainable Energy Rev* 175: 113183(1-20). https://doi.org/10.1016/j.rser.2023.113183
5. Wall M (2024) *Watch this private Varda Space capsule's blistering return to Earth in amazing onboard video.* Space Exploration. Available from: https://www.space.com/varda-in-space-manufacturing-capsule-earth-return-video
6. Krakos A (2024) Lab-on-chip technologies for space research — current trends and prospects. *Microchimica Acta* 191: 31(1-21).
7. Kuang S, Sign N, Wu Y, Shen Y, Ren W, Tu L, et al. (2022) Role of microfluidics in accelerating new space missions. *Biomicrofluidics* 16: 021503. https://doi.org/10.1063/5.0079819
8. Nakamura K, Takayanagi T, Sato S (1989) Modified Arrhenius equation. *Chem Phys Lett* 160: 295–298.
9. Visscher V, van der Schaaf J, Nijhuis T, Schouten JC (2013) Rotating reactors - a review. *Chem Eng Res Design* 91: 1929–1940. https://doi.org/10.1016/j.cherd.2013.07.021
10. Qui Z, Zhao L, Weatherley L (2010) Process intensification technologies in continuous biodiesel production. *Chem Eng Processing: Proc Intensification* 49: 323–330. https://doi.org/10.1016/j.cep.2010.03.005
11. Cihonski J, Gulliver E (2014) Rapid preparation of pharmaceutical intermediates and targets using process intensification. *Pharmaceuticals* June 2004: 8–12.
12. Hampton PD, Wealton MD, Roberts LM, Yaeger AA, Boydson R (2008) Continuous organic synthesis in a spinning tube-in-tube reactor: TEMPO-catalysed oxidation of alcohols by hypochlorite. *Org Process Res Dev* 12: 946–949. https://doi.org/10.1021/op800051t
13. Gonzales M, Ciszewski J (2009) High conversion, solvent-free, continuous synthesis of imidazolium ionic liquids in spinning tube-in-tube reactors. *Org Process Res Dev* 13: 64–66. https://doi.org/10.1021/op8001917
14. Andereck C, Liu S, Swinney H (1986) Flow regimes in a circular Couette system with independently rotating cylinders. *J Fluid Mechanics* 164: 155–183. https://doi.org/10.1017/S0022112086002513
15. Loupy A (Ed.) (2006) *Microwaves in Organic Synthesis*, Weinheim: Wiley-VCH. https://doi.org/10.1002/9783527619559
16. Kappe C, Stadler A, Dallinger D, (2012) *Microwaves in Organic and Medicinal Chemistry*, Weinheim: Wiley-VCH. https://doi.org/10.1002/3527606556
17. Khaghanikavkani E, Farid M, Holdem J, Williamson A (2013) Microwave pyrolysis of plastic. *J Chem Eng Process Techn* 4: 1000150(1-11). https://doi.org/10.1016/j.crcon.2023.03.002
18. Kouzaev G, Kapranov S (2015) Scalable reactor for microwave- and ultrasound-assisted chemistry, UK Patent Application # GB1504690.7 dated 19.03.2015. *IPO Searchable Patents J* 6572: May 6, 2015.

19. Mitani T, Hasegawa N, Nakajima R, Shinohara N, Nozaki Y, Chikata T, et al. (2016) Development of a wideband microwave reactor with a coaxial cable. *Chem Eng J* 299: 209–216. https://doi.org/10.1016/j.cej.2016.04.064
20. Kapranov S, Kouzaev G (2018) Nonlinear dynamics of dipoles in microwave electric field of a nanocoaxial tubular reactor. *Molecular Physics* 117: 489–506. https://doi.org/10.1080/00268976.2018.1524526
21. Kapranov S, Kouzaev G (2019) Study of microwave heating of reference liquids in a coaxial waveguide reactor using experimental, semi-analytical, and numerical means. *Int J Thermal Sci* 140: 505–520. https://doi.org/10.1016/j.ijthermalsci.2019.03.023
22. Kouzaev G, Kapranov V (2020) Microwave miniature coaxial reactors for on-demand material synthesis. *TechRxiv Preprint*. https://doi.org/10.36227/techrxiv.11649678.v2
23. Sarabi F, Chorbani M, Stankiewicz A, Nigar H (2020) Coaxial traveling-wave microwave reactors: Design challenges and solutions. *Chem Eng Research Design* 153: 677–683. https://doi.org/10.1016/j.cherd.2019.11.022
24. Topcam H, Karatas O, Erol B, Erdogdu F (2020) Effect of rotation on temperature uniformity of microwave processed low-high viscosity liquids: A computational study with experimental validation. *Innov Food Sci Emerging Techn* 60: Article No. 103306. https://doi.org/10.1016/j.ifset.2020.102306
25. Miyakawa M, Kanamori S, Hagihara K, Itagaki A, Nakamura T, Nishioka M (2021) Cylindrical resonator-type microwave heating reactor with real-time monitoring function of dielectric property applied to drying processes. *Industr Eng Chem Res* 60: 9119–9127. https://doi.org/10.1021/acs.iecr.1c00569
26. Shi WD, Wang C, Yang WC (2022) Model-based design and operation of coaxial-type microwave reactor toward large-scale production of nanoparticles. *Chem Eng Sci* 264: Article No. 118162. https://doi.org/10.1016/j.ces.2022.118162
27. Sharma G, Kouzaev G (2023) Miniature glass-metal coaxial waveguide reactors for microwave-assisted liquid heating. *AIMS Electro Electri Eng* 7: 100–120. https://doi.org/10.3934/electreng.2023006
28. Kouzaev G (2022) Glass-metal coaxial-waveguide reactors for on-demand microwave-assisted chemistry. *TechRxiv Preprint*. https://doi.org/10.36227/techrxiv.20045006.v2
29. Kouzaev G (2017) A method and apparatus for separate supply of microwave and mechanical energies to liquid reagents in coaxial rotating chemical reactors. *UK Patent Appl. GB2560545A* dated 15.03.2017. *IPO Searchable Patents J* 6675: April 26 2017. https://patentimages.storage.googleapis.com/5f/6d/c2/cae7c780904d53/GB2560545A.pdf
30. Hur D, Say M, Diltemiz S, Duman F, Ersöz A, Say R (2018) 3D micropatterned all-flexible microfluidic platform for microwave-assisted flow organic synthesis. *ChemPlusChem* 83: 42–46.
31. Gregory A, Clarke R (2012) Tables of the complex permittivity of dielectric reference liquids at frequencies up to 5 GHz. *NPL Report Mat 23*: 87 p.
32. Kapranov S, Kouzaev G (2018) Models of water, methanol, and ethanol and their applications in the design of miniature microwave heating reactors. *Int J Thermal Sci* 122: 53–73. https://doi.org/10.1016/j.ijthermalsci.2017.08.007
33. Kouzaev G (2023) Thin-film rotating coaxial reactor for microwave-assisted rapid chemistry *TechArxiv Preprint*. https://doi.org/10.36227/techrxiv.24718350.v1

Appendix

Table 1A. Commercially available parts, instruments, and materials used in experiments and their main parameters.

No	Notations in the text	Part name	Manufacturer/seller	Parameters
1	Dielectric rotor 1	Alumina tube	*E-Bay*	99% Al_2O_3, ε_r = 9.9, OD = 7 mm, ID = 3.7 mm, L_R = 204 mm
2	Dielectric rotor 2	Fused quartz (SiO_2) tube	*Lianyungang Highborn Technology Co., Ltd.*	ε_r = 3.78, OD = 6.96 mm, ID = 4.18 mm, L_R = 204 mm
3	Electromotor	SE30RR2NTC	*Minebea*	24 V, 8000 rpm, max
4	Sealed coaxial connector	BM 60807	*Bracke Manufacturing*	N female 1" panel mount hermetically sealed connector with O-ring
5	MW generator	KU SG 2.45-250A, signal generator	*Kuhne Electronics. Microwave Components*	Frequency: 2.45 GHz; output power: 0–250 W, 10 W step
6	Reflectometer	ZDP-BN 35691	*Rohde&Schwartz*	Frequency range: 300 MHz–4.2 GHz
7	Coaxial cables to power meters, 0.5 m	Interconnect coaxial cable Sucoflex 104P	*Huber+Suhner*	Attenuation: <0.5 dB m^{-1}
8	PM-I	Power meter NRP-Z22	*Rohde&Schwartz*	Frequency range: 10 MHz–18 GHz
9	PM-R	Power meter MA24126A	*Anritsu*	Frequency range: 10 MHz–26 GHz
10	A_1	Attenuator MCL	*Microcircuits*	Inserted loss: 20 dB
11	A_2	Attenuator MCL	*Microcircuits*	Inserted loss: 10 dB
12	Coaxial cable from generator to reactor, 1 m	Interconnect coaxial cables Sucoflex 404	*Huber+Suhner*	Attenuation: <0.5 dB m^{-1}
13	Pump	Peristaltic dispensing pump LP-BT100-1F/DG-4(10)	*Drifton*	Speed: 0.1–100 rpm.
14	Tubing	Tygon MHSL 2001	*Drifton*	OD = 4.49 mm, ID = 2.7 mm
15	O-TM	Fiber optic temperature transmitter FTX-100-LUX+ and fiber optic sensor PRB-G-40	*Osensa Innovations*	Temperature resolution: 0.01 ℃
16	Mini non-contact tachometer UNI-T	48883	*Uni-trend Technology*	Portable device, laser technology
17	Detector	Microwave leakage detector professional H-M2	*Amazon*	Frequency: 2.450 GHz
18	C_2H_5OH	Ethanol	*Kiilto*	98% purity

19	CH_3OH	Methanol	*VWR*	95% purity
20	VNA	Network analyzer NanoVNA V2 Plus4 Pro	*HCXQS group*	Bandwidth: 50 kHz–4 GHz